Brain Structure and Degeneration Staging in Friedreich Ataxia: Magnetic Resonance Imaging Volumetrics from the ENIGMA-Ataxia Working Group

Ian H. Harding, PhD,[1,2] Sidhant Chopra, BSc,[2,3] Filippo Arrigoni, MD,[4] Sylvia Boesch, MD,[5] Arturo Brunetti, MD,[6] Sirio Cocozza, MD,[6] Louise A. Corben, PhD,[3,7,8] Andreas Deistung, PhD,[9,10] Martin Delatycki, PhD,[7] Stefano Diciotti, PhD,[11] Imis Dogan, PhD,[12,13] Stefania Evangelisti, PhD,[14] Marcondes C. França Jr PhD, MD,[15,16] Sophia L. Göricke, MD,[17] Nellie Georgiou-Karistianis, PhD,[3] Laura L. Gramegna, MD,[14,18] Pierre-Gilles Henry, PhD,[19] Carlos R. Hernandez-Castillo, PhD,[20,21] Diane Hutter, RN,[19] Neda Jahanshad, PhD,[22] James M. Joers, PhD,[19] Christophe Lenglet, PhD,[19] Raffaele Lodi, PhD, MD,[14,23] David N. Manners, PhD,[14] Alberto R. M. Martinez, PhD,[15,16] Andrea Martinuzzi, PhD, MD,[24] Chiara Marzi, PhD,[11] Mario Mascalchi, PhD, MD,[25,26] Wolfgang Nachbauer, PhD, MD,[27] Chiara Pane, MD,[28] Denis Peruzzo, PhD,[4] Pramod K. Pisharady, PhD,[19] Giuseppe Pontillo, MD,[6,29] Kathrin Reetz, MD,[12,13] Thiago J. R. Rezende, PhD,[15,16] Sandro Romanzetti, PhD,[12,13] Francesco Saccà, MD,[28] Christoph Scherfler, MD,[5,30] Jörg B. Schulz, MD,[12,13] Ambra Stefani, MD,[5] Claudia Testa, PhD,[31] Sophia I. Thomopoulos, BA,[22] Dagmar Timmann, MD,[10] Stefania Tirelli, MSc,[4] Caterina Tonon, PhD, MD,[14,18] Marinela Vavla, PhD, MD,[24] Gary F. Egan, PhD,[2,3†] and Paul M. Thompson, PhD[22†]

Objective: Friedreich ataxia (FRDA) is an inherited neurological disease defined by progressive movement incoordination. We undertook a comprehensive characterization of the spatial profile and progressive evolution of structural brain abnormalities in people with FRDA.

View this article online at wileyonlinelibrary.com. DOI: 10.1002/ana.26200

Received Feb 15, 2021, and in revised form Aug 19, 2021. Accepted for publication Aug 21, 2021.

Address correspondence to Dr Harding, Department of Neuroscience & Monash Biomedical Imaging, Monash University, Melbourne, VIC 3800, Australia. E-mail: ian.harding@monash.edu

†G.F.E. and P.M.T. contributed equally.

From the [1]Department of Neuroscience, Central Clinical School, Monash University, Melbourne, VIC, Australia; [2]Monash Biomedical Imaging, Monash University, Clayton, VIC, Australia; [3]School of Psychological Sciences, Turner Institute for Brain and Mental Health, Monash University, Clayton, VIC, Australia; [4]Neuroimaging Unit, Scientific Institute, IRCCS Eugenio Medea, Bosisio Parini, Italy; [5]Department of Neurology, Medical University of Innsbruck, Innsbruck, Austria; [6]Department of Advanced Biomedical Sciences, University of Naples Federico II, Naples, Italy; [7]Bruce Lefroy Centre, Murdoch Children's Research Institute, Parkville, VIC, Australia; [8]University of Melbourne, Parkville, VIC, Australia; [9]University Clinic and Outpatient Clinic for Radiology, Department for Radiation Medicine, University Hospital Halle (Saale), Halle (Saale), Germany; [10]Department of Neurology, Essen University Hospital, University of Duisburg-Essen, Essen, Germany; [11]Department of Electrical, Electronic, and Information Engineering "Guglielmo Marconi,", University of Bologna, Bologna, Italy; [12]Department of Neurology, RWTH Aachen University, Aachen, Germany; [13]JARA-BRAIN Institute, Molecular

Methods: A coordinated international analysis of regional brain volume using magnetic resonance imaging data charted the whole-brain profile, interindividual variability, and temporal staging of structural brain differences in 248 individuals with FRDA and 262 healthy controls.
Results: The brainstem, dentate nucleus region, and superior and inferior cerebellar peduncles showed the greatest reductions in volume relative to controls (Cohen $d = 1.5–2.6$). Cerebellar gray matter alterations were most pronounced in lobules I–VI ($d = 0.8$), whereas cerebral differences occurred most prominently in precentral gyri ($d = 0.6$) and corticospinal tracts ($d = 1.4$). Earlier onset age predicted less volume in the motor cerebellum ($r_{max} = 0.35$) and peduncles ($r_{max} = 0.36$). Disease duration and severity correlated with volume deficits in the dentate nucleus region, brainstem, and superior/inferior cerebellar peduncles ($r_{max} = -0.49$); subgrouping showed these to be robust and early features of FRDA, and strong candidates for further biomarker validation. Cerebral white matter abnormalities, particularly in corticospinal pathways, emerge as intermediate disease features. Cerebellar and cerebral gray matter loss, principally targeting motor and sensory systems, preferentially manifests later in the disease course.
Interpretation: FRDA is defined by an evolving spatial profile of neuroanatomical changes beyond primary pathology in the cerebellum and spinal cord, in line with its progressive clinical course. The design, interpretation, and generalization of research studies and clinical trials must consider neuroanatomical staging and associated interindividual variability in brain measures.

ANN NEUROL 2021;00:1–14

Friedreich ataxia (FRDA) is the most common hereditary ataxia.[1] It is caused by biallelic mutations in the *FXN* gene, resulting in transcriptional repression of the "frataxin" protein, leading to abnormal mitochondrial bioenergetics.[2] The characteristic progressive neurological abnormalities of FRDA include ataxia of gait and limbs, dysarthria, and dysphagia. Symptoms typically first manifest around puberty, although onset can occur anytime from infancy through to midlife. FRDA has a disabling, unrelenting, and currently untreatable course leading to premature mortality.[3]

In the nervous system, primary neuropathology targets the dorsal root ganglia and dorsal horns of the spinal cord, the dentate nuclei of the cerebellum, and the spinocerebellar and corticospinal tracts.[4,5] The neuropathology of FRDA is thought to result from a combination of abnormal development and progressive degeneration, whereas spinal cord and brainstem changes may predominantly arise due to abnormal developmental processes, and cerebellar and cerebral changes likely follow a more progressive course.[5,6]

Magnetic resonance imaging (MRI) has increasingly been used to localize, quantify, and track in vivo anatomical brain changes in people with FRDA. Early, robust, and progressive volume loss in the dentate nuclei has been reported,[7–9] although in the cerebellar cortex the detection and localization of volume loss has varied markedly across studies.[9–14] In the brainstem, regions corresponding to the spinocerebellar and dentatothalamic tracts show particularly marked volumetric changes that correlate with disease severity, onset age, and duration.[7,8,14–16] Although the cerebral cortex is generally thought to be anatomically spared in FRDA, mild cortical thinning and reduced volume in the primary motor and somatosensory cortices, premotor regions, and occipital/calcarine areas have been variously reported.[11,17] Evidence of volume loss and microstructural changes in the corticospinal tracts is also robust, and widespread white matter injury has been reported throughout much of the cerebrum and corpus callosum.[8,12,14,15]

Taken together, available literature supports the utility of noninvasive neuroimaging to characterize and track brain changes in FRDA, and potentially to address the urgent need for reliable treatment monitoring and stratification biomarkers for clinical trials. However, due to the rarity of FRDA, MRI studies to date have examined modestly sized cohorts (median cohort size = 21, range = 8–37, in 22 studies published from 2008 to 2020), limiting statistical power, reliability, generalizability, and

Neuroscience and Neuroimaging, Research Center Jülich, Jülich, Germany; [14]Department of Biomedical and Neuromotor Sciences, University of Bologna, Bologna, Italy; [15]Department of Neurology, School of Medical Sciences, University of Campinas, Campinas, Brazil; [16]Brazilian Institute of Neuroscience and Neurotechnology, School of Medical Sciences, University of Campinas, Campinas, Brazil; [17]Institute of Diagnostic and Interventional Radiology and Neuroradiology, Essen University Hospital, University of Duisburg-Essen, Essen, Germany; [18]IRCCS Institute of Neurological Sciences of Bologna, Functional and Molecular Neuroimaging Unit, Bologna, Italy; [19]Department of Radiology, Center for Magnetic Resonance Research, University of Minnesota, Minneapolis, MN; [20]Faculty of Computer Science, Dalhousie University, Halifax, NS, Canada; [21]CONACYT–Institute of Neuroethology, University of Veracruz, Xalapa, Mexico; [22]Imaging Genetics Center, Mark and Mary Stevens Institute for Neuroimaging and Informatics, Keck School of Medicine, University of Southern California, Marina del Rey, CA; [23]IRCCS Institute of Neurological Sciences of Bologna, Bologna, Italy; [24]Scientific Institute, IRCCS Eugenio Medea, Conegliano–Pieve di Soligo Research Center, Conegliano, Italy; [25]Department of Clinical and Experimental Biomedical Sciences "Mario Serio,", University of Florence, Florence, Italy; [26]Clinical Epidemiology Unit, ISPRO, Oncological Network, Prevention and Research Institute, Florence, Italy; [27]Medical University of Innsbruck, Innsbruck, Austria; [28]NSRO Department, University of Naples Federico II, Naples, Italy; [29]Department of Electrical Engineering and Information Technology, University of Naples Federico II, Naples, Italy; [30]Neuroimaging Research Core Facility, Medical University of Innsbruck, Innsbruck, Austria; and [31]Department of Physics and Astronomy, University of Bologna, Bologna, Italy

Additional supporting information can be found in the online version of this article.

opportunities to examine factors that affect disease variability. Key questions also remain regarding the temporal staging and dynamic profile of brain changes in FRDA. Heterogeneous clinical phenotypes and rates of symptom progression are observed as a factor of early (<15 years) relative to late (>25 years) commencement of symptoms.[3,18] Moreover, there are clear differences in the temporal trajectory of the disease in the first few decades compared to the later years.[19] However, it remains unclear whether this variability reflects properties of the clinical scales, or true differences in the neuropathological progression of FRDA, and efforts to characterize any neuroanatomical substrates underpinning this clinical variability are nascent.[14,17]

The ENIGMA-Ataxia working group was formed to address these open questions through multisite aggregation and coordinated analyses of MRI data (http://enigma.ini.usc.edu/ongoing/enigma-ataxia/). Here, we aim to undertake a comprehensive evaluation of whole-brain structure in individuals with FRDA relative to healthy controls (CONT), including identification of early versus late disease characteristics and the influence of childhood compared with adolescent and adult symptom onset.

Subjects and Methods

Participants and Data

We employed a cross-sectional design based on retrospective multisite data aggregation, with coordinated prospective analysis of all data. Data from 248 individuals with FRDA and 262 age- and sex-matched CONT from across 10 research sites were included (Table). Individuals with FRDA were genetically confirmed to have biallelic mutations in intron 1 of the *FXN* gene (GAA repeat expansions on both alleles, n = 243; one expanded allele and one point mutation, n = 5). Data collection, analysis, and contributions to this project were governed by the human research ethics body at each site as previously published and/or defined here: Aachen (RWTH Aachen University project EK 083/15),[16] Bologna,[20] Campinas,[14] Conegliano (IRCCS Eugenio Medea, project 155/CE-Medea),[12] Essen (Essen University Hospital, project 15-6404-BO), Florence,[21] Innsbruck (Medizinische Universität Innsbruck, project 1074/2017), Melbourne (Monash Health, project #13201B),[15] Minnesota (University of Minnesota, STUDY00009047), and Naples (University of Naples Federico II, project 47/15).[13] Multisite data aggregation and analysis were approved by the Monash University Human Research and Ethics Committee (project #12372). All data were fully anonymized prior to aggregation, including assignment of new subject identifier codes.

Age at disease onset was defined as the age at first symptom expression, and disease duration as the time from onset to MRI examination. Disease severity was quantified using one of the following validated clinical scales: the Friedreich Ataxia Rating Scale, the Scale for Assessment and Rating of Ataxia, or the International Cooperative Ataxia Rating Scale (see Supplementary Table S1). Higher scores on these scales indicate greater clinical severity. The retrospective nature of the study precluded clinical phenotyping using a common scale. Due to the distinct psychometric properties of these different scales, and the potential for systematic differences in the implementation of

TABLE. Participant Demographics across the 10 Study Sites

	Friedreich Ataxia					Control		
Site	n	Female, n (%)	Age	Disease Duration	Onset Age	n	Female, n (%)	Age
Aachen	26	12 (46)	36.3 (12.2)	19.7 (9.6)	16.7 (7.7)	35	20 (57)	35.2 (13.2)
Bologna	17	9 (53)	29.4 (12.8)	20.5 (11.4)	8.9 (4.7)	15	9 (60)	31.3 (10.1)
Campinas	52	33 (63)	29.8 (13.6)	11.6 (9.2)	18.3 (9.4)	61	37 (61)	29.5 (13.3)
Conegliano	39	20 (52)	22.9 (11.3)	11.6 (8.0)	11.3 (7.1)	23	13 (57)	27.7 (9.01)
Florence	17	9 (53)	32.4 (9.7)	14.2 (8.2)	18.2 (9.1)	21	11 (52)	32.1 (7.18)
Innsbruck	13	6 (46)	46.0 (12.3)	20.3 (9.1)	25.7 (12.2)	18	7 (39)	45.7 (12.5)
Essen	15	9 (60)	44.1 (11.3)	22.7 (8.5)	21.4 (7.2)	14	8 (57)	42.4 (14.1)
Melbourne	31	14 (45)	36.5 (13.0)	17.0 (9.5)	19.5 (8.8)	37	17 (46)	37.1 (12.8)
Minnesota	19	10 (53)	18.5 (7.4)	4.7 (3.1)	13.8 (5.8)	18	8 (44)	21.4 (6.75)
Naples	19	6 (32)	28.4 (14.1)	11.6 (7.0)	17.1 (9.9)	20	9 (45)	29.4 (9.75)
Total[a]	248	128 (52)	31.1 (14.0)	14.5 (9.79)	16.7 (9.20)	262	139 (53)	32.7 (12.9)

Age, disease duration, and onset age are reported in mean years (standard deviation).

[a]There were no statistically significant differences ($p > 0.05$) between individuals with Friedreich ataxia and controls in age or sex, across all sites.

the same scale across sites, disease severity scores were not directly aggregated between sites, as described in the Statistical Analysis section below.

The MRI data used in this study consisted of high-resolution T1-weighted anatomical images collected on 3T (8 sites) or 1.5T (2 sites) clinical scanners at a voxel size of no greater than $1mm^3$ (Supplementary Table S2). All images collected at each site were acquired using the same scanner and protocol; data were available for both cohorts (FRDA and CONT) from all sites.

Image Processing

Spatially Unbiased Infratentorial Toolbox for Cerebellar Gray Matter. Cerebellar gray matter volume was quantified using the Spatially Unbiased Infratentorial Toolbox (SUIT) v3.2 (www.diedrichsenlab.org/imaging/suit.htm) and SPM12 (https://www.fil.ion.ucl.ac.uk/spm/software/spm12/). Default settings from SUIT 3.2 were used, with the exception of tissue modulation using the affine component of the template registration in addition to the default modulation based only on the nonlinear warp (see further details below). Subtentorial structures (ie, cerebellum and brainstem) were first isolated from the rest of the brain and segmented to produce gray matter partial-volume images. The subtentorial masks were manually inspected for accuracy, and edited to exclude remaining areas of the occipital lobe or surrounding vasculature when necessary. The gray matter partial volume images were then normalized to the SUIT template using a DARTEL registration approach. The images were modulated based on both the affine and nonlinear components of the transformation to preserve volume encoding in the normalized images. The affine transform encodes information related to the overall size and scale of the cerebellum, whereas the nonlinear transform estimates more localized anatomical features. The global changes encoded by the affine transform are often treated as confounds resulting from variability of noninterest (eg, head size), and are thus excluded from consideration during volume estimation. However, in this work, between-group differences in both global and local anatomical features of the cerebellum are expected and are of interest. Both are therefore considered in our voxelwise volume estimates, and variability in head size is accounted for during statistical analysis by covarying for intracranial volume (ICV). For quality control, the spatial covariance (ie, overlap) of each normalized image relative to all others from that site was assessed to identify misregistrations or abnormal image features. Any image in which the average covariance to the rest of the sample fell 2 standard deviations below the site mean was manually inspected and excluded for artifacts or severe motion corruption, but otherwise retained. The images were spatially smoothed using a Gaussian kernel of 3mm full width at half maximum (FWHM).

CAT12 Toolbox for Cerebral Gray Matter and Whole-Brain White Matter. Cerebral gray matter and whole-brain white matter were quantified with the Computational Anatomy Toolbox (CAT12 v12.5; http://www.neuro.uni-jena.de/cat/) and SPM12 implemented in MATLAB. Standard (default) settings from CAT12 v12.5 were used, with the exception that the final tissue maps were written out in 1mm (as opposed to 1.5mm) isotropic voxels. In brief, each image underwent bias-field correction, skull stripping, segmentation into gray and white matter, and normalization to Montreal Neurological Institute space using the DARTEL algorithm. Voxel-level intensities for each white and gray matter image were modulated by the Jacobian determinants derived during both linear and nonlinear spatial normalization to preserve volume encoding. The resulting normalized and modulated gray and white matter images were spatially smoothed using a 5mm Gaussian kernel at FWHM. Spatial covariance quality control was performed as above. The cerebellum was masked out of the gray matter images prior to spatial smoothing to prevent signal contamination across the tentorium. Total ICV was quantified as the sum of gray matter, white matter, and cerebrospinal fluid volumes using CAT12 segmentations.

Adjustment for Site Effects and Healthy Aging Prior to Disease-Related Correlations. Variability in volume estimation may be introduced by systematic differences between sites (eg, technical considerations related to different scanners and MRI acquisition sequences; or differences in cohort characteristics) and/or the effect of aging (eg, healthy aging and disease progression).

In our between-group inference, this variance is of noninterest and is accounted for by inclusion of appropriate regressors in the linear model (see Statistical Analysis). However, in the estimation of associations between brain volume and disease-related measures, it is desirable to control for the influence of site effects and healthy aging, while retaining disease-related variability. Site effects at each voxel were quantified as the difference between the global mean of all CONT across all sites ($\text{mean}_{\text{global\_hc}}$) and the mean of the CONT at each site ($\text{mean}_{\text{site\_hc}}$):

$$\text{image}_{\text{sitecorr}} = \text{image}_{\text{orig}} + \left(\text{mean}_{\text{global\_hc}} - \text{mean}_{\text{site\_hc}}\right)$$

Additional healthy aging effects were estimated using a simple linear regression of current age onto volume at each voxel across all CONT (β_{age}), and used for correction of the FRDA data to the mean age of the sample (ie, expected volume if all subjects were approximately 30 years old) prior to undertaking clinical correlations:

$$\text{image}_{\text{agecorr}} = \text{image}_{\text{sitecorr}} - \left(\beta_{age} * \left[\text{age}_{\text{current}} - \text{age}_{\text{mean}}\right]\right)$$

Statistical Analysis

FRDA versus CONT Between-Group Differences. Between-group differences were estimated using analysis of covariance models, controlling for site, cohort by site, ICV, sex, age, symptom onset age, and disease duration. Inference within the cerebellar gray, cerebral gray, and whole-brain white matter masks was undertaken using both atlas-based and voxel-based approaches. For atlas-based analyses, the mean volume was calculated across all voxels in each region of the Harvard–Oxford cortical and subcortical gray matter atlases and Johns Hopkins University cortical white matter tractography atlas from the FMRIB Software Library (fsl.fmrib.ox.ac.uk, v6.0), the van Baarsen cerebellar white matter atlas,[22] and the SUIT atlas of cerebellar gray matter lobules and dentate nuclei.[23,24] The SUIT dentate nucleus atlas encompasses the full iron-rich "bean-shaped" region, including both the gray matter ribbon and central white matter hilum. As it is not possible to define the boundaries of the dentate nucleus using T1-weighted images, this atlas is also limited to providing a probabilistic localization of this structure. We therefore refer to this area as the "dentate region" of the cerebellar subcortex throughout this article. Inference was not undertaken in lobule X of the SUIT atlas due to inconsistent segmentations of the gray matter in this small structure during image processing. Final inference was Bonferroni familywise error (FWE)-corrected to conservatively control for multiple comparisons ($p_{\text{FWE}} < 0.05$).

Voxel-based analyses were performed in SPM12. Heteroscedasticity was estimated and corrected using a standard restricted maximum likelihood approach implemented in SPM12. Inference was undertaken across all voxels using Gaussian random field theory to consider spatial correlations in the data and provide stringent voxel-level corrections of alpha significance thresholds to account for multiple comparisons (voxel-$p_{\text{FWE}} < 0.05$).

Effect size estimates (Cohen d) were calculated by converting the t statistic of the between-group predictor variable from the regression models, providing an effect size estimate after accounting for known variance of non-interest (eg, site, age).[25]

Disease Correlations and Staging. Volume estimates from the FRDA cohort were assessed for linear relationships with disease duration, onset age, and disease severity. After adjustment for healthy aging and site effects (see above), voxel-level analyses within each of the cerebellar gray, cerebral gray, and white matter masks were undertaken through multiple regression with disease duration, onset age, and ICV modeled as independent variables (ie, disease duration effects while controlling for onset age, and vice versa). Final voxel-level inference was reported as described above. Partial correlation effect sizes (r values) were calculated by converting the relevant t statistics from the regression models.[25]

As multiple clinical scales were used to assess disease severity across sites, a direct pooled analysis (ie, a mega-analysis) was not possible. In this case, a meta-analysis approach was instead employed to identify evidence for associations between clinical severity and brain volume irrespective of the instrument used. First, linear regression of disease severity and ICV on voxel volume was undertaken within each tissue mask for each site individually using SPM12. Second, voxel-based meta-analyses were implemented using the Seed-Based d Mapping software (SDM v6.21; http://www.sdmproject.com). Briefly, SDM implements a voxelwise random-effects meta-analysis on the thresholded t statistic maps from each site. The procedure considers sample size, intrastudy variance, and inter-study heterogeneity. Permutation testing was used for statistical inference at the voxel level, with FWE correction (voxel-$p_{\text{FWE}} < 0.05$).

Qualitative visualizations were also generated to illustrate the evolution of structural brain changes across time (cross-sectionally) and the moderating effects of disease onset age. Subgroups were defined using arbitrary cutoffs of onset age and duration to provide a relative balance in the number of images across subgroups and, where feasible, conform to categories used in previous literature (eg, typical onset, <15 years; intermediate onset, 15–24 years; late onset, >24 years[3,18]). However, these delineations do not necessarily map onto clinically meaningful cutoffs (eg, disability stages), and serve only to aid qualitative data descriptions and interpretations. Effect size maps were calculated for each subgroup relative to a common control cohort (after correction for age and site effects), and are presented at a threshold of Cohen $d > 0.5$ (ie, "medium" effect size) for direct qualitative comparison.

Results

Volumetric Differences in FRDA Relative to CONT (Atlas-Based)

Atlas-based spatial maps of significant effects, and forest plots of effect sizes across regions are illustrated in Fig 1 and tabulated in Supplementary Table S3. The largest and most consistent loss of brain volume in individuals with FRDA is seen in the subtentorial white matter, with strong involvement of the medulla (Cohen $d = 2.6$), midbrain ($d = 1.9$), and pons ($d = 1.5$), the superior

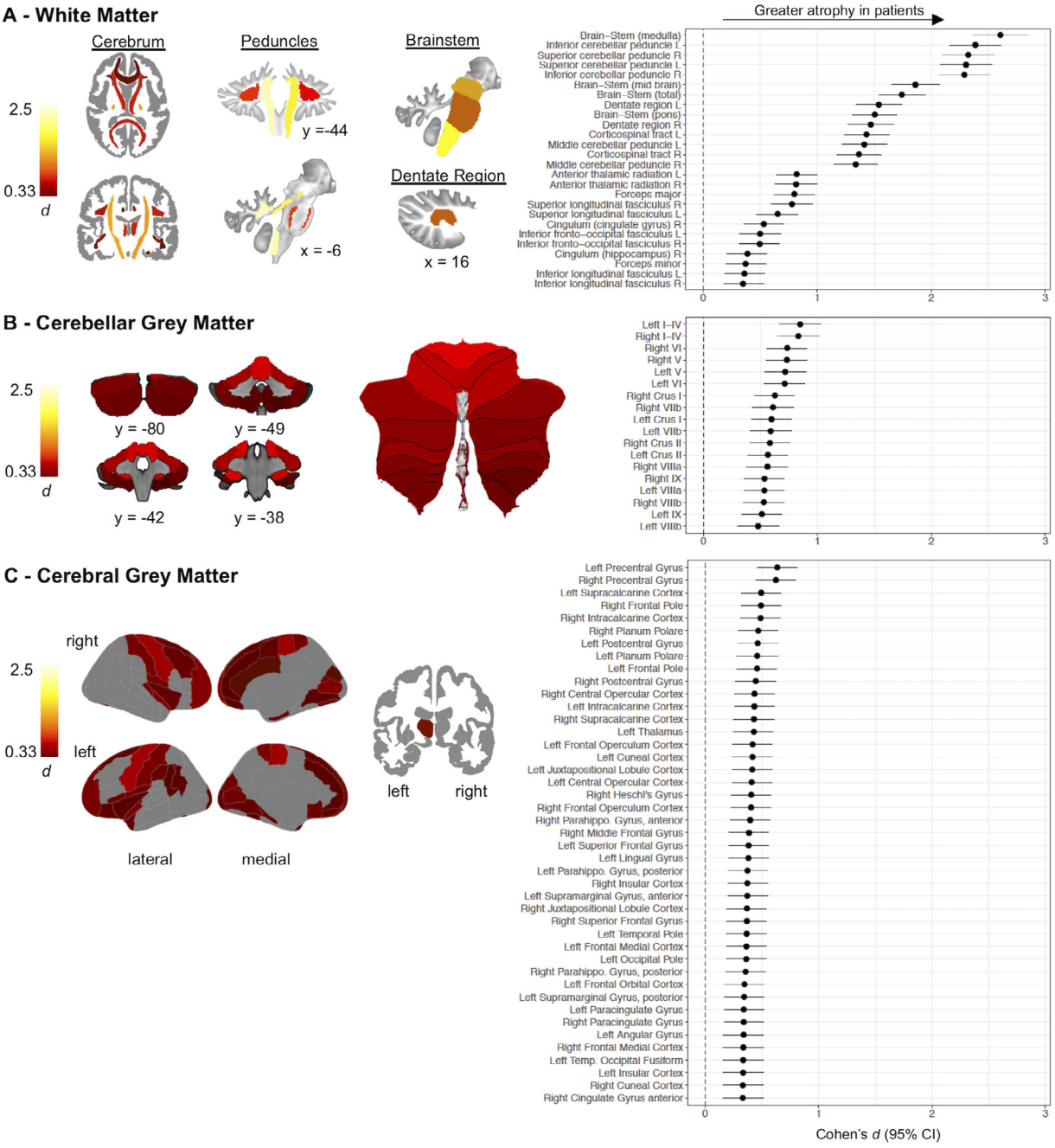

FIGURE 1: Atlas-based effect size (Cohen *d*) maps and forest plots (Cohen *d* ± 95% confidence interval [CI]) for individuals with Friedreich ataxia versus controls, statistically controlling for site, intracranial volume, sex, age, disease onset, and disease duration. Regions with $p_{FWE} < 0.05$ are shown (see Supplementary Table S3 for full tabulation). (A) Cerebral white matter regions of interest (ROIs) were defined using the Johns Hopkins University white matter tractography atlas, and cerebellar white matter ROIs were defined using the van Baarsen cerebellar white matter atlas. (B) Cerebellar gray matter ROIs were defined using the Spatially Unbiased Infratentorial Toolbox cerebellar atlas. (C) Cerebral gray matter ROIs were defined using the Harvard–Oxford cortical and subcortical atlases. Slice coordinates are in Montreal Neurological Institute space.

cerebellar peduncles (SCP) and inferior cerebellar peduncles (ICP; $d > 2.3$), and the dentate region ($d > 1.5$; see Fig 1A, Supplementary Table S3). The corticospinal tracts and middle cerebellar peduncles are also notably impacted ($d > 1.3$). More modest ($0.3 < d < 0.8$) effects are also observed in association and commissural tracts throughout the cerebral white matter.

Reduced gray matter volume in individuals with FRDA is also observed in all cerebellar lobules (see Fig 1B). The strongest effects occur in lobules I–IV, V, and VI ($0.71 < d < 0.85$). More modest effect sizes are seen across the remainder of the posterior lobules ($0.48 < d < 0.63$; see Fig 1B, Supplementary Table S3).

Cerebral involvement is most notable in the bilateral precentral gyri (primary motor areas; $d = 0.62$–0.64; see Fig 1C, Supplementary Table S3). Significant between-group effects are also evident in the primary somatosensory cortices and premotor areas, throughout the medial frontal, orbitofrontal, and opercular/insular cortices, and within visual, cuneal, and fusiform regions ($0.33 < d < 0.49$; see Fig 1C, Supplementary Table S3). Reduced volume in the left thalamus ($d = 0.43$) is also observed, with changes in the right thalamus ($d = 0.31$) failing to reach statistical significance.

Peak Effects and Between-Site Variability (Voxel-Based)

Voxel-based maps and forest plots of effect sizes across sites are presented in Fig 2 and Supplementary Tables S3 and S4. The voxel-level analyses provide finer-grained spatial identification of peak effects. Group differences in the white matter are maximal in the SCP and adjacent cerebellar white matter (peak $d = 2.8$). Voxel-level results also clearly distinguish the globally greater strength of effects in subtentorial (cerebellar/brainstem) relative to supratentorial (cerebral) structures (see Fig 2A). In the cerebral white matter, areas underlying motor and/or somatosensory regions are preferentially impacted. White matter volume loss within these regions is found consistently across sites with medium to large effect sizes (see Fig 2A, Supplementary Table S4).

In the cerebellar gray matter, voxel maps indicate greater nonuniformity of atrophy patterns than indicated in the atlas-based results, but recapitulate the more subtle involvement of cerebellar gray relative to white matter (see Fig 2B). Peak volume loss is observed in lobules I–IV

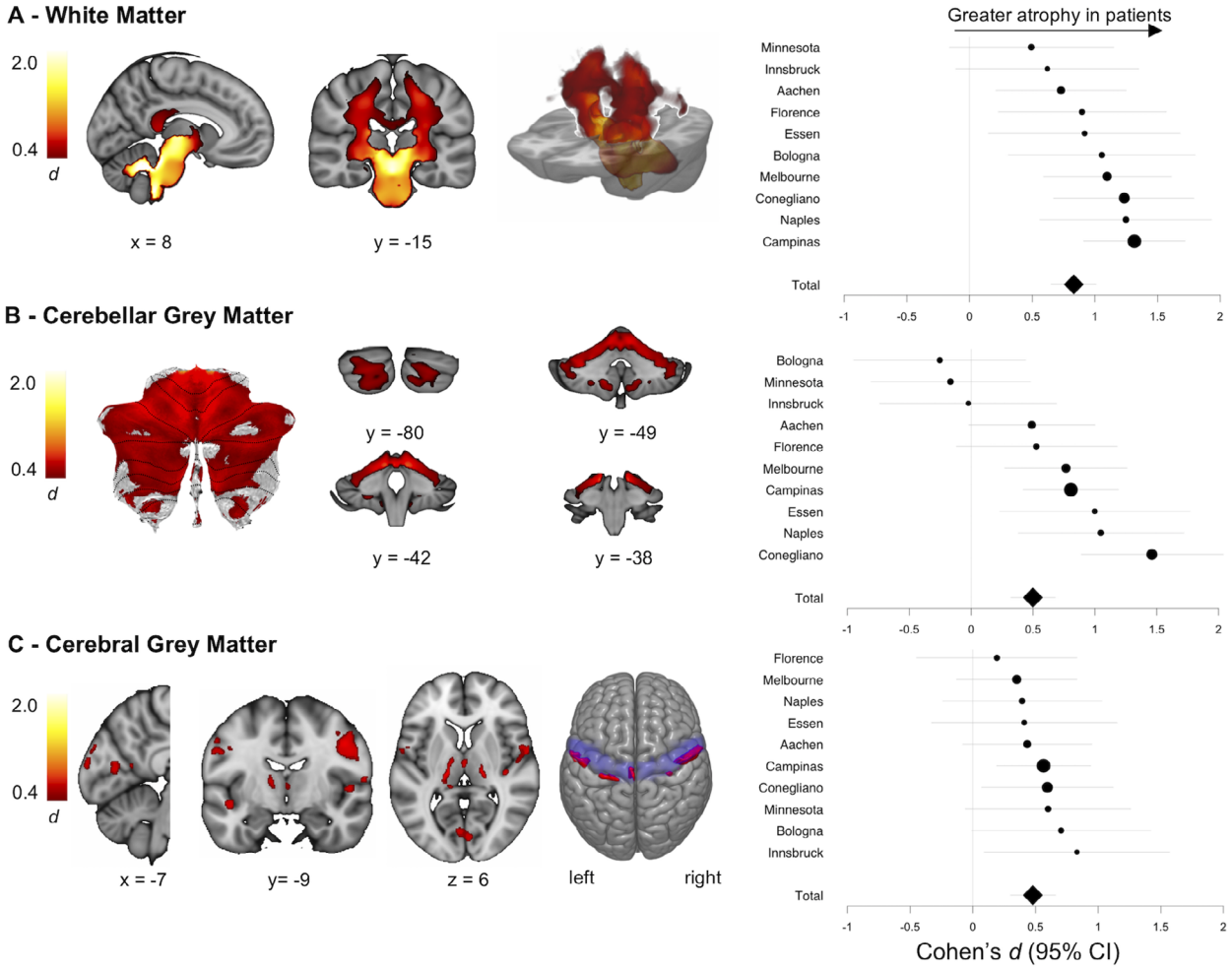

FIGURE 2: Voxel-level effect size (Cohen *d*) maps of individuals with Friedreich ataxia versus controls, statistically controlling for site, intracranial volume, sex, age, disease onset, and disease duration. Only voxels that survive voxelwise $p_{FWE} < 0.05$ are displayed. Forest plots of mean effect size within these regions (Cohen $d \pm 95\%$ confidence interval [CI]) for each site are given on the right, and the size of the point estimate is proportional to the sample size of the site (Supplementary Table S4). (A) White matter (cerebral and cerebellar). (B) Cerebellar gray matter. (C) Cerebral gray matter. The primary motor cortex (precentral gyri) is depicted on the superior surface. Slice coordinates are in Montreal Neurological Institute space. [Color figure can be viewed at www.annalsofneurology.org]

(peak $d = 0.98$) and lobule VI (peak $d = 0.76$). A rescaled version of the cerebellar gray matter map is provided in Fig 3 to more clearly depict the spatial variability of effects. Between-site variability within the study-wide between-group difference mask is evident, with 3 sites showing no effects (on average across the mask), 6 sites showing medium effects, and 1 site showing a large effect (see Fig 2B, Supplementary Table S4).

Significant areas of voxel-level volume loss in the cerebral cortex are highly focal, with strongest effects in the precentral gyri (peak $d = 0.66$) and adjacent areas of the postcentral gyri (see Fig 2C). Using a finer-grained cerebral atlas,[26] these effects are further sub-localized to bilateral upper limb, head, and face regions, and the left lower limb area (Fig 4). Other areas of voxel-level cortical volume reductions include right Heschl's gyrus/central operculum and bilateral planum polare, frontal operculum, intracalcarine cortex, occipital pole, and parahippocampal gyri (see Supplementary Table S3). Bilateral effects in lateral regions of the thalamus are also

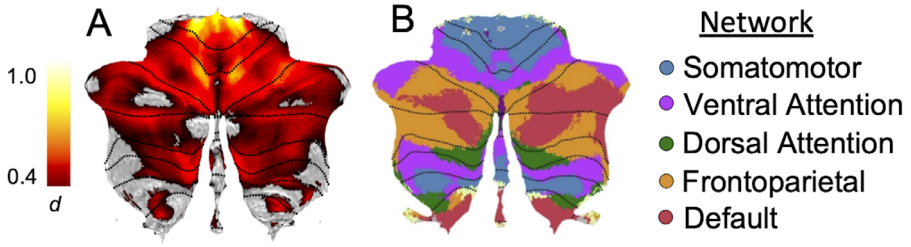

FIGURE 3: Network mapping of between-group changes in the cerebellar cortex (Spatially Unbiased Infratentorial Toolbox template). Peak anatomical changes are localized to the somatomotor network, with hot spots also evident in the ventral attention network. (A) The effect size map is rescaled from Fig 2B to more easily depict the spatial pattern of cerebellar effects. (B) The network parcellation is reproduced from Buckner et al 2011.[27] See Supplementary Table S5 for quantification. [Color figure can be viewed at www.annalsofneurology.org]

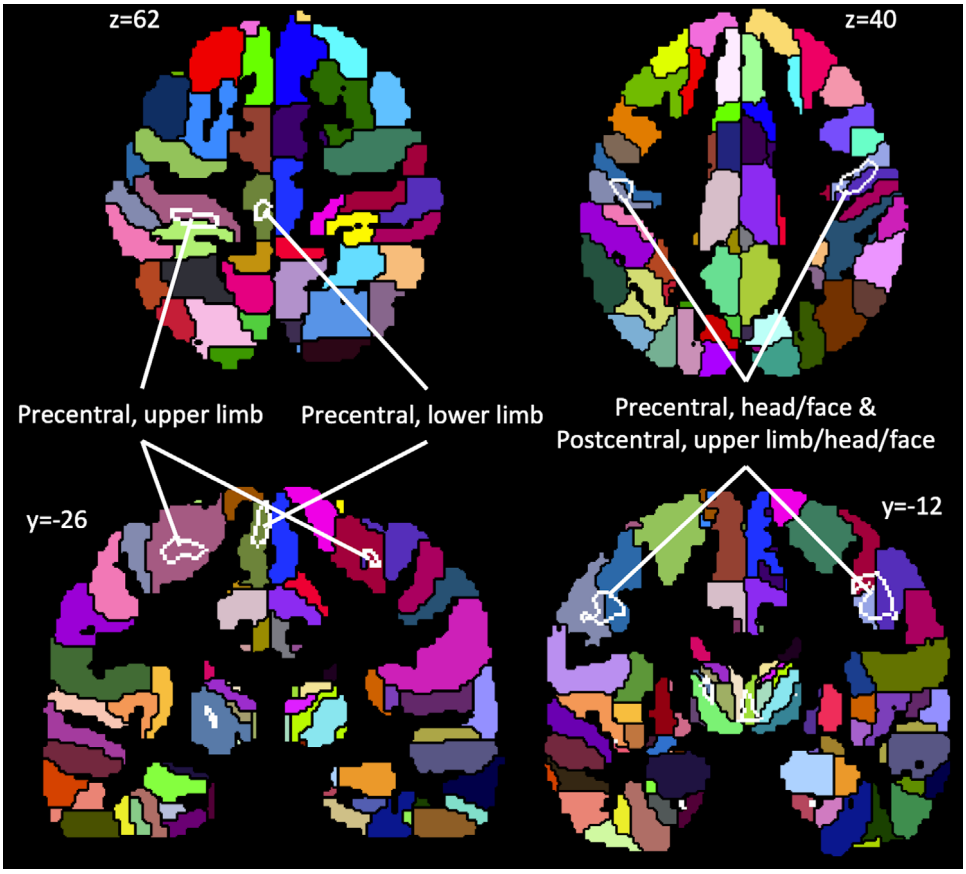

FIGURE 4: Volume decreases in the primary motor and somatosensory cortices (Fig 2C) are further disambiguated using a finer parcellation of the cortex provided by the Brainnetome Atlas. Areas of significant volume loss are shown by white outlines, and labeled according to the atlas. This depiction implicates principal involvement of limb and head regions.

observed (peak $d = 0.76$). Between-site variability within the precentral gyri is relatively constrained, with all sites reporting an effect of $d = 0.6 \pm 0.2$ (see Fig 2C, Supplementary Table S4).

Network Representation of Anatomical Changes

Mapping of the correspondence between structural differences and brain networks was undertaken by characterizing the profile of volumetric changes within an atlas of brain networks defined using functional neuroimaging (see Fig 3, Supplementary Table S5).[27] In the cerebellum, peak effects are located in the somatomotor network ($d_{peak} = 0.95$), and significant between-group effects are evident in more than half of the voxels (55.7%) comprising this network. Large proportions of the frontoparietal, dorsal attention, and ventral attention networks are also impacted (39–46% of voxels reaching statistical significance), whereas anatomical changes in areas ascribed to the default mode network are less abundant (28%; see Supplementary Table S5). In the cerebrum, peak effects are also located in the somatomotor cortex, although a much smaller proportion of the full network is implicated (4.7%). Small areas of the visual and ventral attention cerebral networks are also affected (1.1–1.5%).

Correlations with Disease Onset, Duration, and Severity

Significant negative linear correlations with disease duration (controlling for onset age and healthy aging), indicative of less volume with greater disease duration, are evident throughout the white matter of the cerebellum and brainstem, the cerebellar gray matter in bilateral lobule VI, crus I, and right lobule VIIIa, the bilateral thalamus, and the left middle frontal gyrus (Fig 5, Supplementary Table S6).

Onset age (controlling for duration and healthy aging) is correlated with white matter volume, indicative of less volume in individuals with younger onset, in dentate regions of the cerebellum, the SCP, and the ICP. In the cerebellar cortical gray matter, less volume with earlier onset is observed, particularly in bilateral lobule I–IV, and VIIIb/IX (see Fig 5, Supplementary Table S6). There are no significant effects in cerebral regions.

Finally, the meta-analysis indicated that disease severity negatively correlates with volume, indicating lower volume in individuals with more severe neurological symptoms, throughout much of the cerebellar cortex and white matter, with strongest effects in lobules I–IV, VI, and IX and crus I,

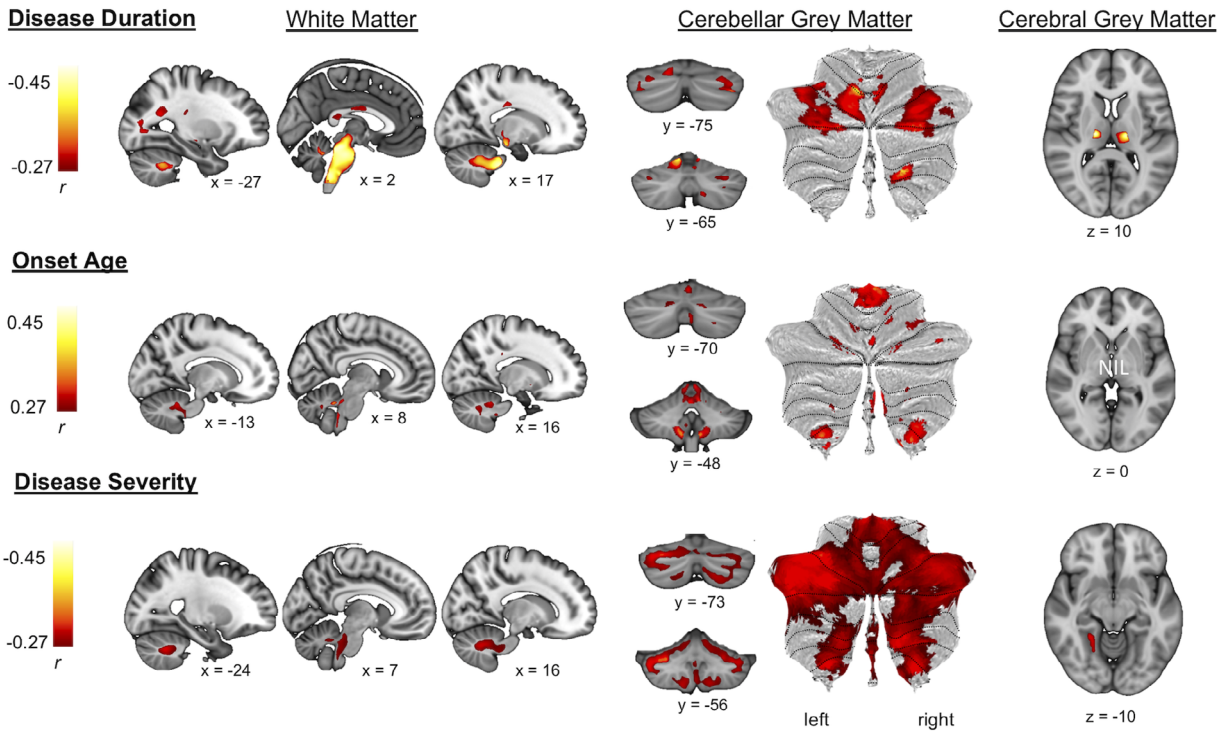

FIGURE 5: Voxel-level correlation maps (partial *r*) between tissue volume and disease duration (negative), age at disease onset (positive), and disease severity (negative) for patients with Friedreich ataxia. Only voxels that survive voxel-level $p_{FWE} < 0.05$ are depicted. Disease duration correlations were computed using voxel-level regression while adjusting the model for disease onset age, current age, site, and intracranial volume (ICV). Disease onset correlations were also computed using voxel-level regression while adjusting the model for disease duration, age, site, and ICV. For correlations with disease severity, voxel-based meta-analysis was employed to account for the use of different clinical scales across sites. See Supplementary Table S6 for full tabulation. Slice coordinates are in Montreal Neurological Institute space. [Color figure can be viewed at www.annalsofneurology.org]

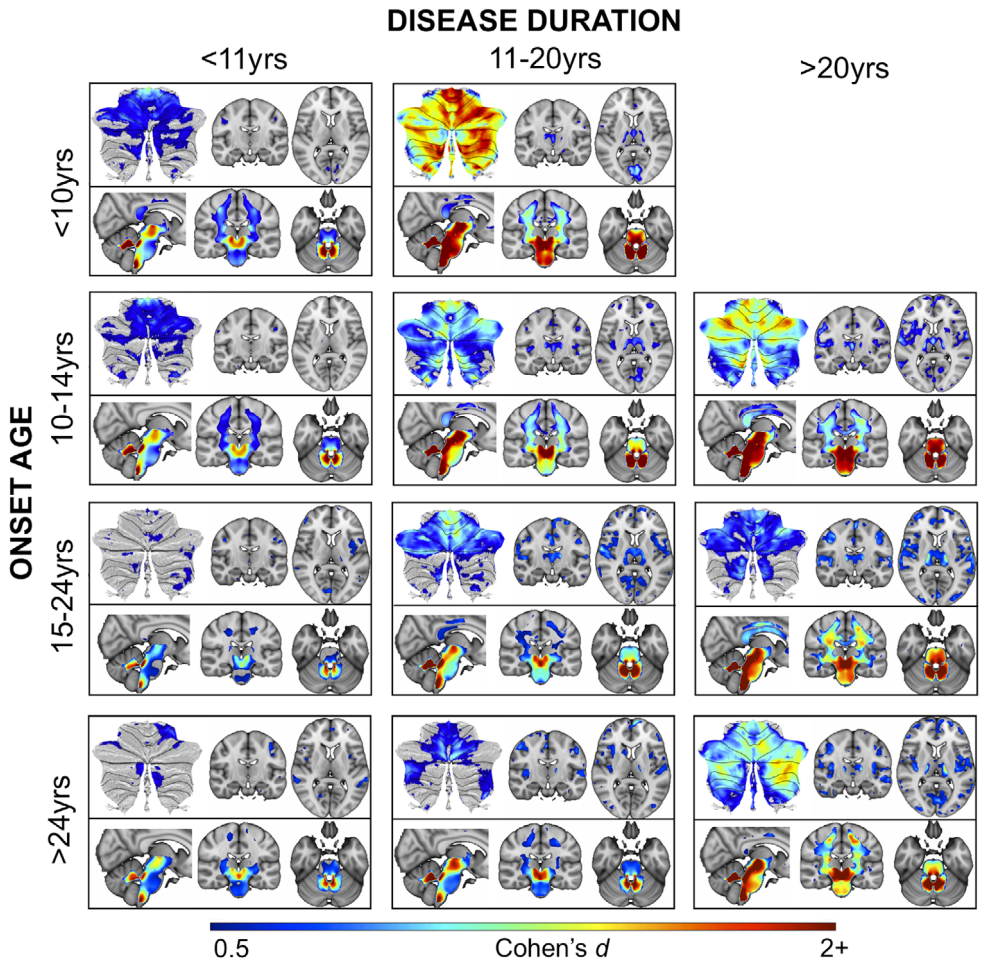

FIGURE 6: Subgroup effect size maps (Cohen *d* > 0.5) relative to the full control cohort (adjusted for age and site), demonstrating disease staging and the moderating role of onset age on brain structure. For each subgroup, gray matter effects are displayed on top (cerebellum flat map and representative cerebrum coronal and axial slices), and white matter effects on the bottom (representative sagittal, coronal, and axial slices). There are no data presented in the top right quadrant due to insufficient data in this subcohort. See Supplementary Table S7 for subgroup sizes and demographics.

and throughout the white matter and dentate regions (see Fig 5, Supplementary Table S6). A significant correlation is also evident in the left lingual gyrus.

Qualitative representations of volumetric changes in subgroups of individuals with FRDA, stratified according to disease duration and onset age, are presented in Fig 6. Each subgroup comprises between 15 and 38 individuals (see Supplementary Table S7 for subgroup characteristics). Data from the SCP and dentate region, representing the areas of greatest between-group differences and strongest correlations with all clinical variables, are plotted in Fig 7. The volume data are *z*-normalized relative to the control distribution ($[mean_{FRDA} - mean_{CONT}] / std\_deviation_{CONT}$).

Discussion

We performed a large-scale, coordinated analysis of structural brain MRI data from individuals with FRDA (and CONT) from 10 sites across the globe, yielding a comprehensive characterization of volumetric brain differences. Volumetric differences were most pronounced in subtentorial white matter areas corresponding to the brainstem, SCP, ICP, and dentate regions of the cerebellar subcortex. These findings are consistent with the established neuropathology of FRDA,[5] as the primary sites of degeneration in the dorsal root ganglia/dorsal columns of the spinal cord and the dentate nuclei of the cerebellum give rise to the ICP and the SCP, respectively.[4] Reduced volume in these regions was also found to be an early, progressive, and universal (across subgroups) feature of FRDA and was associated with clinical severity and disease duration. Volume deficits in the brainstem and cerebellar subcortex are thus core features of FRDA, and volumetric measures of the SCP and dentate regions in particular represent excellent candidates for longitudinal follow-up and validation as T1-weighted MRI biomarkers in this disease.

Volume loss in white matter at a lesser magnitude was also observed more extensively throughout the brain,

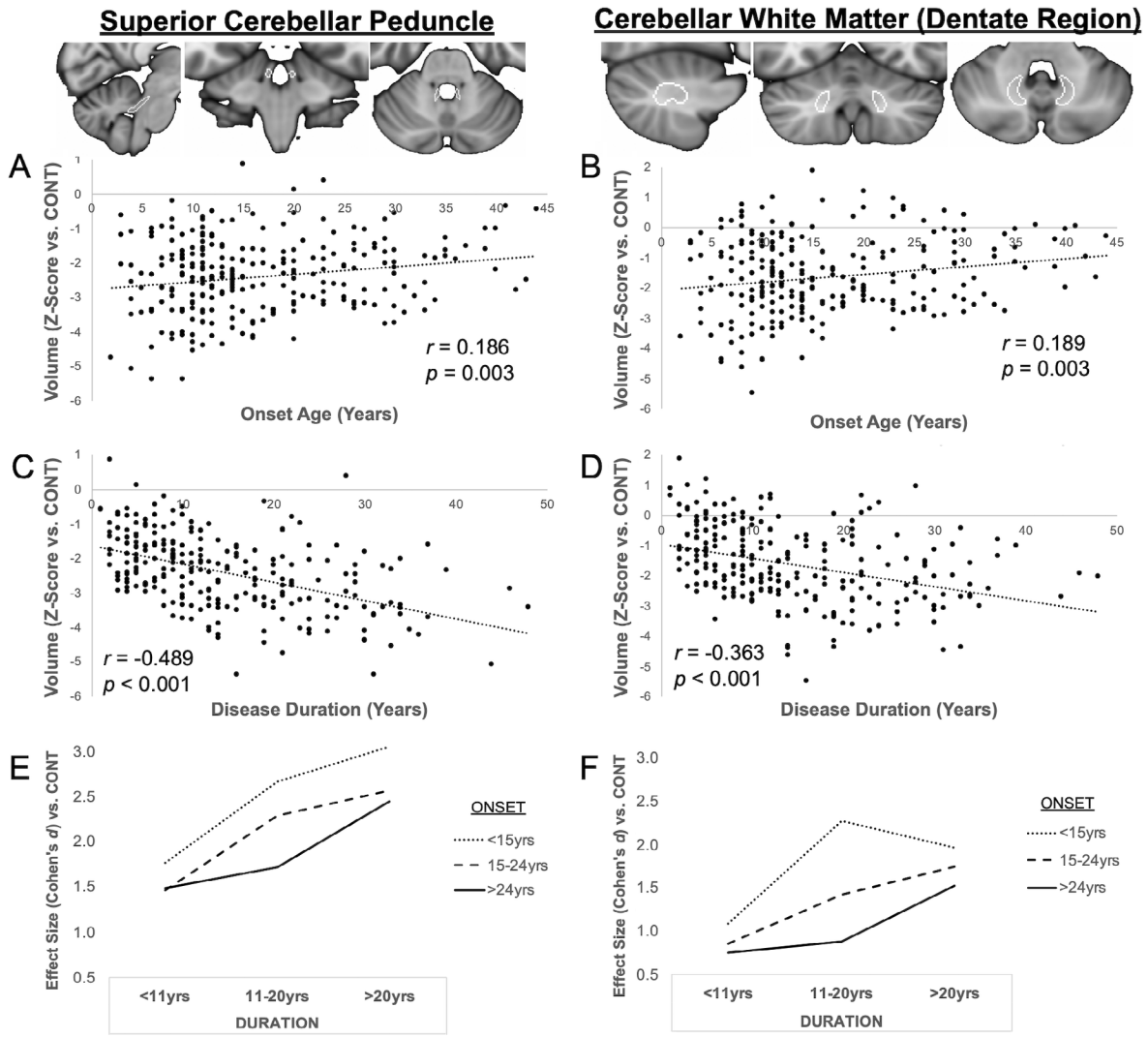

FIGURE 7: Data plots for the bilateral superior cerebellar peduncles (van Baarsen atlas) and cerebellar dentate region (dentate nucleus mask from the Spatially Unbiased Infratentorial Toolbox atlas) in the Friedreich ataxia (FRDA) cohort (age and site adjusted, and *z*-normalized to the control (CONT) data distribution [($mean_{FRDA}$ – $mean_{CONT}$) / $std\_deviation_{CONT}$]). These regions represent the strongest between-group differences relative to controls, with significant correlations with both disease onset age and disease duration, and map onto the primary pathology of FRDA. (A–D) Scatterplots depict linear relationships between volume and each of disease onset age (A, B) and disease duration (C, D); compare to Fig 5. (E,F) Line graphs illustrate effect size estimates across the 9 subgroups; compare to Fig 6).

most notably in the regions corresponding to motor (corticospinal), occipital (forceps major, including the splenium of the corpus callosum), and thalamic (anterior thalamic radiations) tracts. Widespread loss of brain white matter recapitulates the increasing number of single-site MRI reports of similar effects using techniques sensitive to both volumetric and microstructural (eg, diffusion-weighted imaging) changes.[28] Although the current study cannot elucidate the mechanisms driving these changes, these subcortical effects can only partially be explained as secondary axonal degeneration resulting from primary pathology in "core" disease regions.

Gray matter abnormalities occur more mildly than the strongest white matter effects, but more extensively than recognized in contemporary disease descriptions. Anatomical differences in the cerebellar cortex are weighted toward the anterior lobe and adjacent areas, whereas smaller effect sizes are evident throughout the posterior lobe. Anterior lobe cerebellar damage is known to result preferentially in motor impairments, whereas posterior lobe damage produces a cognitive and affective syndrome.[29] Cerebral changes similarly manifest preferentially in primary motor and somatosensory regions, alongside small effects in opercular, occipital, and other prefrontal areas (including visual and auditory cortices). These findings are consistent with the clinical profile of FRDA, which is defined by robust motor and somatosensory deficits alongside milder and more variable cognitive, affective, visual, and auditory symptoms.[3,30]

Cross-sectional trends and cohort subgrouping revealed important insights into disease staging and inter-individual variability in FRDA. Reduced volume in the dentate nucleus region, SCP, ICP, and midbrain white matter are early and progressive disease features. Conversely, atrophy in the thalamus, cerebellar cortex, cerebral white matter, and cerebral cortex increasingly manifest with greater disease duration. Importantly, the pattern and extent of this progressive degeneration differ by disease onset age. Individuals with childhood or early adolescent onset generally have a longer GAA1 (smaller allele) repeat expansion in *FXN*, resulting in less frataxin production and a more aggressive clinical progression.[2] Here, we show that these individuals also have earlier and more extensive cerebellar gray matter, brainstem, and cerebral white matter involvement. In comparison, in individuals with later symptom onset, which is associated with slower progression and a qualitatively milder clinical phenotype, cerebellar involvement is milder and does not manifest consistently until later in the disease course, particularly in the posterior lobe. Additionally, individuals with younger disease onset show early degeneration in cerebellar motor areas (lobules I–IV and VIIIb), whereas progressive atrophy in cerebellar areas associated with premotor and cognitive functions (lobules VI and VIIIa, crus I) is more universal. The mechanisms driving increased vulnerability of the motor cerebellum in individuals with earlier disease onset are unclear. One possibility is that motor impairments that manifest in childhood may have a secondary impact on the continuing maturation of motor control systems. In this case, interruption of developmental trajectories, in addition to progressive degenerative processes, could explain the neuroanatomical and clinical distinctions between this group and adolescent/adult onset individuals who experience onset of motor symptoms and associated cerebellar degeneration after the motor system has reached greater maturity. This hypothesis is a compelling avenue for further investigation. Finally, progressive and mild cerebral involvement is predominantly a late feature of FRDA and does not appear to be modulated by disease onset age.

We demonstrate here that volumetric changes in the dentate region and brainstem are not only consistently evident at the earliest disease stages, but also appear to be features that are most likely to be sensitive to progression irrespective of disease stage, as demonstrated by significant linear relationships with disease duration. Conversely, the pattern of later emergence of anatomical changes suggests changes in these regions may be more relevant to subsequent disease stages, first in cerebellar anterior lobe, thalamus, corticospinal white matter, and cerebral motor regions, and subsequently extending to the cerebellar posterior lobe and more widespread cerebral gray and white matter areas. However, longitudinal data collected from individuals at different points in the disease course will be necessary to investigate whether the rate of atrophy in different brain regions is stage-dependent.

The anatomical evolution of FRDA also has important implications for cross-study and between-cohort comparability. In this work, evidence of cerebellar gray matter atrophy was particularly variable across sites. Upon further investigation, sites demonstrating no evidence of cerebellar changes include our cohorts with the shortest average disease duration (Minnesota, 4.7 years) and the oldest average onset age (Innsbruck, 25.7 years). Additionally, the site with the largest cerebellar volumetric differences predominantly enrolled childhood onset cases (Conegliano, average onset age = 11.3 years). These findings are consistent with the overall trends described above, exemplifying the importance of considering disease stratification when characterizing FRDA and the critical need to compare like-for-like cohorts when aggregating evidence across studies. This is also a critical point of consideration in the design of clinical trials, whereby participants at different disease stages would ideally be balanced across treatment arms or stratified into subcohorts (within the bounds of feasibility in a rare disease).

Interestingly, associations between brain structure and disease severity were observed across cerebellar gray and white matter, encompassing both motor and non-motor functional regions of the cerebellar cortex. This observation is consistent with recent work indicating that the severity of cognitive symptoms correlates with the severity of motor symptoms in FRDA.[31] However, the relative contribution of cerebellar cortical changes to disease phenomenology and the causal factors driving this atrophy—as Purkinje cells are shown to be largely spared in FRDA[4]—remain unclear. Although we have shown here that the neuroanatomical profile of FRDA in the brain is widespread, the role of primary pathology (ie, frataxin deficiency) relative to secondary epiphenomena (eg, transneuronal degeneration) in driving these milder and temporally delayed disease features remains a topic for future research.

Several limitations and other associated avenues for further work must be considered. The cross-sectional design presented here supports the progressive nature of structural brain changes in FRDA but cannot provide inference or effect size estimates on intraindividual longitudinal changes. Our analyses are also undertaken using T1-weighted MRI, the most common and widely accessible imaging modality in research and clinical practice. However, the dentate nuclei are not visible on T1-weighted images, so we could not directly assess their

integrity in this work; here, the region encompassing the dentate is subsumed within the cerebellar white matter and a probabilistic atlas is used to infer volume changes in the "dentate region." Novel approaches for imaging the dentate nuclei in FRDA have been undertaken at single sites,[9,32] and opportunities for large-scale data aggregation should be considered in the future. Similarly, although we have explored macroscopic changes in white matter volume, further mechanistic insights may be gained with imaging modalities sensitive to tissue microstructure (eg, diffusion-weighted imaging). Finally, the retrospective, multisite nature of this study prevented more extensive investigation of brain–behavior relationships. In particular, the use of different clinical scales between sites and the universal availability only of composite scores (as opposed to individual scale items) prevented more explicit mapping of different disability stages or specific symptom domains onto different neuroanatomical profiles. We hope that this work will provide a priori targets to investigate specific symptom domains and disability stages in the future.

In summary, this work provides new insights and robust effect size estimates of volumetric brain changes in FRDA, serves as a resource to guide further scientific discovery and clinical trial design, strongly motivates prospective longitudinal research to validate volumetric changes in the SCP and dentate nuclei as biomarkers of disease progression and treatment monitoring, and reveals the benefits of large-scale coordinated studies in the rare disease community.

Acknowledgments

The method harmonization and multisite data analysis elements of this work were supported by the NIH BD2K (Big Data to Knowledge) program (grant U54 EB020403) and the Australian National Health and Medical Research Council (fellowship 1106533, grant 1184403).

Author Contributions

Conception and design of the study and methods: I.H.H., S.Ch., C.R.H.-C., N.J., S.I.T., G.F.E., P.M.T. Acquisition and analysis of data, Aachen: K.R., I.D., S.R., J.B.S.; Bologna: R.L., S.E., C.Te., C.To., D.N.M., L.L.G.; Campinas: M.C.F., T.J.R.R., A.R.M.M.; Conegliano: A.M., F.A., M.V., D.P., S.T.; Essen: D.T., A.D., S.L.G.; Florence: M.M., S.D., C.M.; Innsbruck: S.B., W.N., C.S., A.S.; Melbourne: N.G.-K., I.H.H., L.A.C., M.D., G.F.E.; Minnesota: C.L., P.-G.H., J.M.J., P.K.P., D.H.; Naples: S. Co., F.S., G.P., A.B., C.P. Analysis of multisite data and drafting initial manuscript: I.H.H., S.Ch.

Potential Conflicts of Interest

Nothing to report.

Data Availability

All code, data processing instructions, and group-level effect maps are available at https://github.com/Harding-Lab/enigma-ataxia. All individual-level effect maps (warped, modulated voxel maps for voxel-based morphometry) can be accessed through a secondary data use proposal submitted to the ENIGMA-Ataxia working group (http://enigma.ini.usc.edu/ongoing/enigma-ataxia/).

References

1. Ruano L, Melo C, Silva MC, Coutinho P. The global epidemiology of hereditary ataxia and spastic paraplegia: a systematic review of prevalence studies. Neuroepidemiology 2014;42:174–183.
2. Delatycki MB, Bidichandani SI. Friedreich ataxia—pathogenesis and implications for therapies. Neurobiol Dis 2019;132:104606.
3. Reetz K, Dogan I, Costa AS, et al. Biological and clinical characteristics of the European Friedreich's Ataxia Consortium for Translational Studies (EFACTS) cohort: a cross-sectional analysis of baseline data. Lancet Neurol 2015;14:174–182.
4. Koeppen AH, Mazurkiewicz JE. Friedreich ataxia: neuropathology revised. J Neuropathol Exp Neurol 2013;72:78–90.
5. Harding IH, Lynch DR, Koeppen AH, Pandolfo M. Central nervous system therapeutic targets in Friedreich ataxia. Hum Gene Ther 2020;31:1226–1236.
6. Mascalchi M, Bianchi A, Ciulli S, et al. Lower medulla hypoplasia in Friedreich ataxia: MR imaging confirmation 140 years later. J Neurol 2017;264:1526–1528.
7. Harding IH, Raniga P, Delatycki MB, et al. Tissue atrophy and elevated iron concentration in the extrapyramidal motor system in Friedreich ataxia: the IMAGE-FRDA study. J Neurol Neurosurg Psychiatry 2016;87:1261–1263.
8. Lindig T, Bender B, Kumar VJ, et al. Pattern of cerebellar atrophy in Friedreich's ataxia—using the SUIT template. Cerebellum 2019;18:435–447.
9. Stefanescu MR, Dohnalek M, Maderwald S, et al. Structural and functional MRI abnormalities of cerebellar cortex and nuclei in SCA3, SCA6 and Friedreich's ataxia. Brain 2015;138:1182–1197.
10. Dogan I, Tinnemann E, Romanzetti S, et al. Cognition in Friedreich's ataxia: a behavioral and multimodal imaging study. Ann Clin Transl Neurol 2016;3:572–587.
11. Selvadurai LP, Harding IH, Corben LA, et al. Cerebral and cerebellar grey matter atrophy in Friedreich ataxia: the IMAGE-FRDA study. J Neurol 2016;263:2215–2223.
12. Vavla M, Arrigoni F, Nordio A, et al. Functional and structural brain damage in Friedreich's ataxia. Front Neurol 2018;9:747.
13. Cocozza S, Costabile T, Pontillo G, et al. Cerebellum and cognition in Friedreich ataxia: a voxel-based morphometry and volumetric MRI study. J Neurol 2020;267:350–358.
14. Rezende TJR, Martinez ARM, Faber I, et al. Developmental and neurodegenerative damage in Friedreich's ataxia. Eur J Neurol 2019;26:483–489.
15. Selvadurai LP, Corben LA, Delatycki MB, et al. Multiple mechanisms underpin cerebral and cerebellar white matter deficits in Friedreich ataxia: the IMAGE-FRDA study. Hum Brain Mapp 2020;41:1920–1933.

16. Dogan I, Romanzetti S, Didszun C, et al. Structural characteristics of the central nervous system in Friedreich ataxia: an in vivo spinal cord and brain MRI study. J Neurol Neurosurg Psychiatry 2019;90: 615–617.

17. Rezende TJR, Martinez ARM, Faber I, et al. Structural signature of classical versus late-onset Friedreich's ataxia by multimodality brain MRI. Hum Brain Mapp 2017;38:4157–4168.

18. Rummey C, Corben LA, Delatycki MB, et al. Psychometric properties of the Friedreich Ataxia Rating Scale. Neurol Genet 2019;5:371.

19. Tai G, Corben LA, Gurrin L, et al. A study of up to 12 years of follow-up of Friedreich ataxia utilising four measurement tools. J Neurol Neurosurg Psychiatry 2015;86:660–666.

20. Gramegna LL, Tonon C, Manners DN, et al. Combined cerebellar proton MR spectroscopy and DWI study of patients with Friedreich's ataxia. Cerebellum 2017;16:82–88.

21. Della Nave R, Ginestroni A, Giannelli M, et al. Brain structural damage in Friedreich's ataxia. J Neurol Neurosurg Psychiatry 2008;79: 82–85.

22. van Baarsen KM, Kleinnijenhuis M, Jbabdi S, et al. A probabilistic atlas of the cerebellar white matter. Neuroimage 2016;124:724–732.

23. Diedrichsen J, Balsters JH, Flavell J, et al. A probabilistic MR atlas of the human cerebellum. Neuroimage 2009;46:39–46.

24. Diedrichsen J, Maderwald S, Kuper M, et al. Imaging the deep cerebellar nuclei: a probabilistic atlas and normalization procedure. Neuroimage 2011;54:1786–1794.

25. Nakagawa S, Cuthill IC. Effect size, confidence interval and statistical significance: a practical guide for biologists. Biol Rev Camb Philos Soc 2007;82:591–605.

26. Fan L, Li H, Zhuo J, et al. The human brainnetome atlas: a new brain atlas based on connectional architecture. Cereb Cortex 2016;26: 3508–3526.

27. Buckner RL, Krienen FM, Castellanos A, et al. The organization of the human cerebellum estimated by intrinsic functional connectivity. J Neurophysiol 2011;106:2322–2345.

28. Selvadurai LP, Harding IH, Corben LA, Georgiou-Karistianis N. Cerebral abnormalities in Friedreich ataxia: a review. Neurosci Biobehav Rev 2018;84:394–406.

29. Stoodley CJ, MacMore JP, Makris N, et al. Location of lesion determines motor vs. cognitive consequences in patients with cerebellar stroke. Neuroimage Clin 2016;12:765–775.

30. Reetz K, Dogan I, Hohenfeld C, et al. Nonataxia symptoms in Friedreich ataxia: report from the registry of the European Friedreich's Ataxia Consortium for Translational Studies (EFACTS). Neurology 2018;91:e917–e930.

31. Naeije G, Rai M, Allaerts N, et al. Cerebellar cognitive disorder parallels cerebellar motor symptoms in Friedreich ataxia. Ann Clin Transl Neurol 2020;7:1050–1054.

32. Ward PGD, Harding IH, Close TG, et al. Longitudinal evaluation of iron concentration and atrophy in the dentate nuclei in Friedreich ataxia. Mov Disord 2019;34:335–343.